

Dynamics of aerosol extinction coefficients and scattered UV-radiation fluxes during the solar eclipse event on the 9th of March, 1997

I.I. Ippolitov, Yu.A. Pkhalagov, M.V. Kabanov, O.V. Ravodina, Z.S. Teodorovich, M.V. Vinarskii, V.N. Uzhegov, N.N. Shchelkanov, and V.N. Genin

*Siberian Physico-Technical Institute at the Tomsk State University
Institute of Atmospheric Optics, Siberian Branch of the Russian Academy of Sciences, Tomsk
Institute of Optical Monitoring, Siberian Branch of the Russian Academy of Sciences, Tomsk*
Received November 20, 1998

Based on an analysis of the data on temporal variability of the sky background-radiation fluxes in the UV, the aerosol extinction coefficients and the atmospheric meteorological parameters obtained during the morning solar eclipse we have found a significant increase in the UV-radiation level during the period of the first minutes after the solar eclipse termination. This effect is shown to coincide in time with the dissipation of fog formed during the solar eclipse. It is supposed that the increase in the scattered UV-radiation flux recorded immediately after the eclipse is due to an addition of the single-scattered direct solar radiation by the particles of the dissipating fog when its vertical optical thickness approaches unity. The estimates presented show that the morning fog formation on the 9th of March was most likely caused by the solar eclipse.

1. Introduction

The investigation of the effect of solar eclipse on the variability of optical characteristics of the Earth's atmosphere is of considerable scientific interest. In particular, a short-time termination of the solar radiation influx during the eclipse and a sharp temperature drop due to this termination have made it possible to assess the rate of condensation processes in the atmosphere when measuring time dependence of the aerosol extinction coefficients. Based on the temporal variability of the UV-radiation flux in the last phase of the solar eclipse and immediately after it the degree of the eclipse influence on the change of the total ozone content (TOC) can be assessed, and with the use of supplementary data it is possible to determine the contribution of other factors to variations of the UV-radiation flux playing a leading part in the protection of life on the Earth.

The favorable conditions for these investigations occurred during the solar eclipse on the 9th of March 1997, which was observed in the eastern part of the northern hemisphere. In the region of Tomsk (56° 30' N and 84° 58' E) the solar eclipse began at 6:56 a.m. (local time) (56 minutes before the sunrise). At the instant of sunrise (7:52 a.m.) the eclipse phase was about 90% and the eclipse maximum phase (94%) was observed at 7:55 a.m. The solar eclipse came to an end at 8:54 a.m. Its duration in Tomsk was 1 hour and 58 minutes.

To study the solar eclipse effect on the optical and meteorological parameters of the atmosphere, simultaneous measurements were made of spectral transmittance of the atmospheric boundary layer and of the scattered solar radiation in the UV region. These measurements were accompanied by the meteorological

observations made at the meteorological station located in the same place and working during these hours in regime of continuous observations.

2. Dynamics of the aerosol extinction coefficients in the atmospheric boundary layer

The measurements of spectral transmittance of the surface layer were carried out on the 9th of March from 7:24 a.m. to 2:00 p.m. (local time) using the instrumental complex described in Ref. 1. The atmospheric transmittance was measured at the wavelengths of 0.44; 0.48; 0.55; 0.69; 0.87; 0.94, and 1.06 μm , which were determined by the interference filters with the halfwidth from 0.006 to 0.015 μm . The measurements were conducted using the scheme with reflection based on the 415 m path (the overall length of the measurement path was 830 m). At every wavelength the signal was averaged over 20 s. The mean time for measuring one spectrum within the range $\lambda = 0.44\text{--}1.06 \mu\text{m}$ was about 5 minutes. The spectral aerosol extinction coefficients $\alpha(\lambda)$ were calculated from the atmospheric transmission spectra obtained using the measurement procedure proposed in Ref. 1.

The characteristic feature of the atmospheric optical situation is that near the measurement site a comparatively dense haze was observed at 7:25 a.m. on the 9th of March (with the visibility range $S_m \approx 6\text{--}8 \text{ km}$) at the relative humidity of air $f = 96\text{--}98\%$ and temperature $t = -14^\circ\text{C}$. Then the haze rapidly thickened and in 10 minutes a very dense fog formed in the atmospheric boundary layer ($S_m < 0.8 \text{ km}$), which was observed during the eclipse. Figure 1 shows the dynamics of spectral aerosol extinction coefficients at the first stage of

the fog formation. The fog formation proceeded very rapidly and at 7:45 a.m. the fog density was such that the signals due to radiation propagated through this path, at all wavelengths, fell down to noise level.

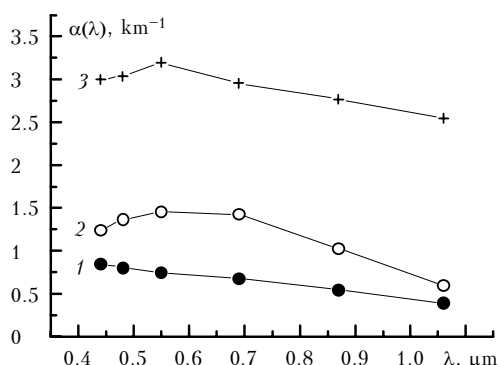


Fig. 1. The dynamics of spectral aerosol extinction coefficients at the first three stages of measurements when passing from haze to fog at 7:25, 7:30, and 7:35 a.m. (local time) (curves 1, 2, and 3, respectively).

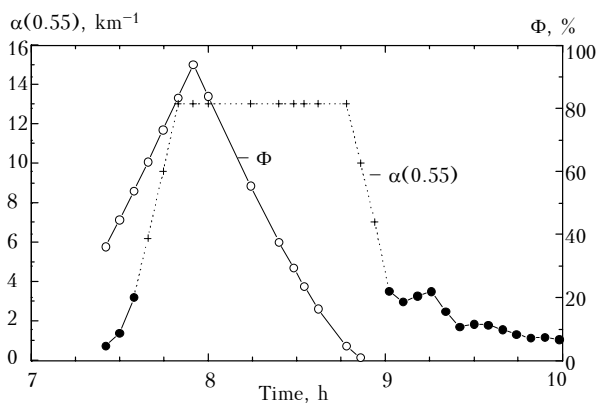


Fig. 2.

Figure 2 shows the time behavior of measured aerosol extinction coefficient $\alpha(0.55)$ and the solar eclipse phase Φ , calculated by the formula

$$\Phi(t) = 94 [1 - \Delta(t)]. \tag{1}$$

Here $\Delta(t)$ is the fraction of open sun disc, which for every instant of time was determined by an approximate formula under the assumption that the apparent diameters (angular dimensions) of the sun and the moon are equal:

$$\Delta(t) = 1 + \frac{2}{\pi} \left[\frac{t}{59} \sqrt{1 - \left(\frac{t}{59}\right)^2} - \arcsin \sqrt{1 - \left(\frac{t}{59}\right)^2} \right], \tag{2}$$

where t is time, in min., which was counted starting from the maximum phase of the eclipse (at 7:55 a.m.).

Time behavior of the coefficient $\alpha(0.55)$ in dense fog, when the signals were at the level of noise, is shown in Fig. 2 by the dashed curve. Over this interval the coefficients were assessed approximately by the known formula $\alpha(0.55) = 3.91/S_m$, where S_m was determined visually using local objects.

The figure shows that the fog began to form intensely ($\alpha(0.55) > 3 \text{ km}^{-1}$) when the eclipse phase was about 50%, and the fog dissipation started practically immediately after the eclipse termination.

Since the above discussed case of the morning fog is the only case in March, it can be assumed that its correspondence to the time limits of the solar eclipse is not an accidental coincidence, but is due to specific features of the thermodynamic processes in the troposphere caused by the solar eclipse. Qualitative analysis of such processes can be made based on the meteorological data over the period from 1:00 a.m. to 4:00 p.m. on the 9th of March 1997, given in the Table 1, where t_1 is the air temperature, t_0 is the temperature of snow surface, e is the partial pressure of water vapor, e_w and e_{ice} denote the pressure of water vapor saturation relative to the water and ice surfaces at the corresponding temperatures.

Table 1.

Measured parameters	Time, h								
	1:00	4:00	7:00	7:30	8:00	8:30	10:00	13:00	16:00
	Type of cloudiness, cloud fraction								
	0/0	10/0, As	10/10, St	10/10, St	fog	fog	10/10, St	10/0, Ci	6/1, Ci, Ac, Sc
$t_0, \text{ }^\circ\text{C}$	-14.2	-20.2	-16.0	-13.5	-13.5	-13.7	-11.2	-4.0	-2.6
$t_1, \text{ }^\circ\text{C}$	-7.2	-11.7	-14.6	-14.0	-13.5	-13.6	-12.6	-7.6	-2.9
$f, \%$	83	99	100	91	93	97	99	87	86
$e, \text{ mb}$	3.02	2.50	1.98	1.98	2.02	2.09	2.32	3.01	4.25
$E_w, \text{ mb}$	3.62	2.52	1.98	2.08	2.16	2.15	2.33	3.46	4.94
$e_{ice}, \text{ mb}$	3.38	2.25	1.71	1.81	1.90	1.88	2.06	3.21	4.80
$B^*, \text{ cal}/(\text{cm}^2\text{-min})$	0.032	-0.030	-0.012	-0.010	-	-	0.005	0.042	-

In the Table 1, for separate time periods, the calculated values of the effective radiation of the Earth's surface b^* are also given. The calculation of b^* was made by the Angström formula² for the case of a clear sky:

$$b^* = \delta(\sigma T_0^4 - a\sigma T_1^4) \tag{3}$$

and for the case when the sky is covered with clouds:

$$b^* = \delta(\sigma T_0^4 - a\sigma T_1^4) - \delta(1 - a) \sigma T_c^4, \tag{4}$$

where $\delta = 0.969$ is the relative infrared radiation absorption coefficient of the Earth's surface; $\sigma = 8.1566 \cdot 10^{-11} \text{ cal}/(\text{cm}^2 \cdot \text{min} \cdot \text{K}^4)$ is the Stefan-Boltzmann constant; $a = K_1 - D \cdot 10^{-ce}$ is the atmospheric emittance coefficient. The following empirical constants K_1 , D , and c were obtained in the calculation: $K_1 = 0.18$; $D = 0.25$ (the dimensionless quantities); $c = 0.95$ (if e_1 has dimensions in mb).

The values of t_0 , t_1 , and e at different moments in time were taken from the Table 1. The values of T_c , corresponding to the temperatures of condensation for the cloudiness of low and medium cloud level, were taken from the mid-latitude thermodynamic model of the atmosphere.³

For following analysis we consider the data given in the Table 1 and in Fig. 3, where, as an example, the time behavior of the air and snow temperature is shown for the period from 1:00 a.m. to 4:00 p.m. on the 9th of March 1997.

It can be seen from Fig. 3, that during the period from 1:00 to 4:00 a.m., in the absence of clouds, the positive effective radiation b^* is observed and the intense radiation cooling of the air and underlying surface took place.

With a decrease in temperature the pressure of water vapor saturation e_w and e_{ice} , reduced that resulted in more intense water vapor precipitation on the snow (by 4:00 $e > e_{ice}$) and in an increased relative humidity of the air. By 4:00 in the morning, due to the formed overcast in the middle and upper cloud levels, the value of b^* became negative, i.e., the incident radiation flux exceeds the leaving one.

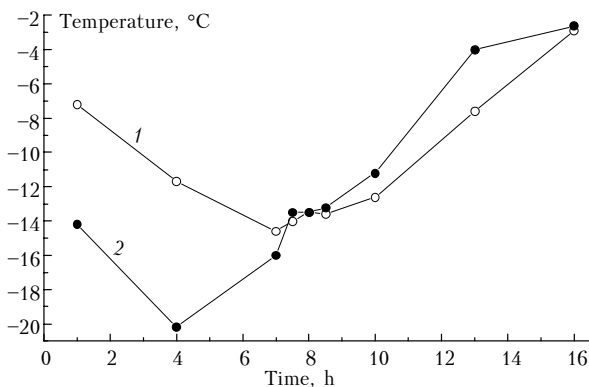


Fig. 3. Time behavior of the air temperature t_1 (curve 1) and of the snow temperature t_0 (2).

Over a period from 4:00 to 7:00 a.m. an interesting situation was observed when the air temperature continues to drop but the snow temperature increases, that is, the snow surface is heated due to the atmospheric radiation reflected backwards. Cooling of the air resulted in the further decrease of e_w and increase of the relative humidity. However the water vapor flow to a colder snow surface prevents the formation of fog in this period.²

The effective radiation b^* over a period from 4:00 to 7:00 a.m. continues to be negative, while decreasing

in magnitude. At about 7:30 a.m. the temperatures of the air and the underlying surface are equal, the water vapor flow to the snow surface stops that, under conditions of high relative humidity of the air (the values of e and e_w are closely related), gave rise to good conditions for the water vapor condensation to begin and thus for fog formation. The latter is the fog of radiation type since at night and in the morning on the 9th of March the weather was calm and no advective transport of air masses was observed.

Based on the optical data (see Fig. 2), the fog was being formed intensely at about 7:35 a.m. that agrees well with the data presented in Fig. 3. The fog dissipation started immediately after the termination of the eclipse as the air warmed up and the water vapor e_w saturation pressure increased.

Thus, the above analysis of time behavior of the atmospheric meteorological parameters as well as of the temperature of underlying surface and the calculated values of b^* indicates that during the eclipse on 9th of March, 1997 the conditions for the occurrence of fog certainly existed. It can be assumed that the occurrence of the overcast serves as the basis for the fog formation. The overcast resulted in a change of sign of the effective atmospheric radiation and favored all the subsequent processes. In its turn the formation of overcast was conditioned by the eclipse when the atmospheric layer height of several kilometers heated by solar radiation coming from below the horizon started to cool off during the eclipse. The cloudiness was formed as a result of processes of moisture condensation in this layer.

3. Dynamics of the scattered UV-radiation fluxes

Measurements of the scattered UV-radiation fluxes were made on 9th and 10th of March 1997 using a filter spectrophotometer⁴ in spectral ranges A and b . The minimum effective spectral sensitivity in the range A was found at $\lambda = 353 \text{ nm}$ with the band halfwidth of 63 nm . The scattered radiation was accumulated from zenith direction by a Quartz hemisphere from the solid angle with the angle at its vertex of 90° . During the eclipse, the readouts were made every minute and every 15 minutes after the termination of the eclipse. Measurements made on the 10th of March may be considered as reference ones. These measurements were carried out under the same meteorological conditions but without the solar eclipse.

If the scattered UV-radiation fluxes in the range A measured on the 9th and 10th of March are denoted by A_9 and A_{10} , then the deviation of the ratio A_9/A_{10} from the unit is connected both with the limitation of the fraction of the open sun ($\Delta = S_{\text{open}}/S_{\text{total}}$) during the eclipse and with the change of atmospheric conditions on these days.

To determine the characteristic properties in the dynamics of the scattered UV-radiation fluxes during the eclipse, the data in Fig. 4 are analyzed where the

time dependence of measured and calculated ratios A_9/A_{10} is given. Curve 2 is calculated by the formula (2) and determines the time dependence of the fraction of the open sun $\Delta(t)$, which in the case of identical atmospheric conditions on the 9th and 10th of March is fully suited to the ratio of fluxes A_9/A_{10} without the account of known effect of the sun disc darkening toward its edges. Curve 3 is calculated with regard for this effect.

The calculation was made by the following formula:

$$\Delta'(t) = \frac{S(\Phi)}{S(0)} = \frac{\int_{322}^{384} I_0(\Phi, \lambda) \exp(-\int_0^{100} \alpha(z, \lambda) dz) d\lambda}{\int_{322}^{384} I_0(0, \lambda) \exp(-\int_0^{100} \alpha(z, \lambda) dz) d\lambda}, \quad (5)$$

where Φ is the eclipse phase; $I_0(\Phi, \lambda)$ denotes the spectral radiation fluxes at the upper atmospheric boundary (100 km) in the range A ($\lambda = 322\text{--}384$ nm) calculated with consideration for the sun disc darkening toward its edges using the methods from Ref. 6; $\alpha(z, \lambda)$ is the volume extinction coefficient, in km^{-1} , at a wavelength λ and at a height z , in km.

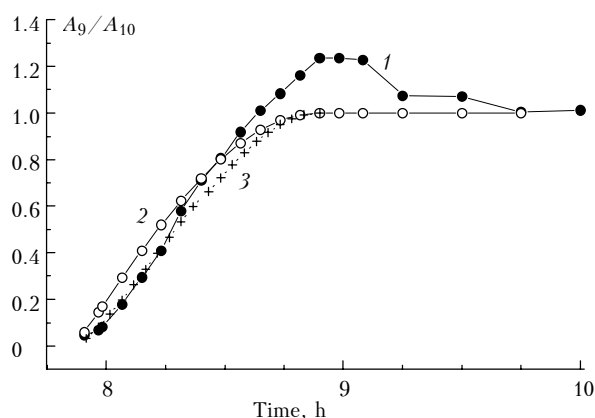


Fig. 4. Time dependence of the ratio of scattered UV-radiation fluxes A_9/A_{10} measured on the 9th and 10th of March (curve 1) and the fraction of the open part of the disk calculated without and with the account of the sun disc limb darkening effect (curves 2 and 3, respectively).

The data on the vertical profiles of the extinction coefficients $\alpha(z, \lambda)$ are taken for the mid-latitude summer of the northern hemisphere from Ref. 3 and the values of $I_0(\Phi, \lambda)$ at the upper atmospheric boundary from Ref. 9. It is evident from the above data that the account for disk limb darkening introduces only insignificant changes of the calculated values of the flux ratio on March 9 and 10.

On the whole, it follows from Fig. 4 that the time behavior of the measured values essentially deviates from the calculated ones and is characterized by a monotonic increase from the moment of sunrise to the maximum of $A_9/A_{10} = 1.24$ corresponding to the

moment of the eclipse termination. Then a decrease in this ratio is observed, the characteristic time is 22 minutes, down to the value $A_9/A_{10} = 1$ with the noticeable deviations from the monotonic behavior.

Much the same pattern for the UV-B range was observed (this pattern is not shown in Fig. 4). Similar maximum of the scattered UV-radiation fluxes at the wavelengths of 315.4 and 323.8 nm in the final phase of the eclipse was also observed in the measurements carried out on March 9, 1997 in Irkutsk.⁵

A pronounced increase of the relative values of the scattered UV-radiation flux immediately after the eclipse is unexpected and calls for the appropriate physical interpretation. Because we consider the time behavior of the ratio of two fluxes measured during different days, then among the possible reasons of a manifestation of this effect may be the distinctions in the total ozone content (TOC), different types of cloudiness or the differences in the optical state of the atmosphere during the above-mentioned days. Now we analyze each specific reason. The fact that the experimental curve at 9:45 a.m. (i.e., in less than an hour after the eclipse termination) reaches the value close to unity enables us to assume that the TOC on the 9th and 10th of March was practically the same. In this connection, it should be assumed that the deviations occurred of the experimental values A_9/A_{10} from the calculated ones in the eclipse closing phase cannot be related to a decrease in the ozone concentration during the eclipse. This conclusion is consistent with the data from Ref. 6, where analysis of the measurement data on TOC was performed for the period of the solar eclipses over a period from 1954 to 1981 and it has been found that the changes in the ozone concentration during the eclipse do not exceed the magnitude of the measurement errors.

The difference in the cloudiness observed on March 9 (overcast of the low-level clouds) and on March 10 (overcast of a medium-level cloud) made a slight impact on the difference between the experimental and calculated values of A_9/A_{10} . This is confirmed by the above-mentioned proximity of the fluxes A_9 and A_{10} shortly after the eclipse termination as well as by the data of many-year investigations,⁷ where it was shown that at low solar angles (5° to 15°), typical for winter months, a transfer from the overcast of low-level clouds to overcast of medium-level and upper-level clouds results in a slight increase ($\sim 5\%$) of the scattered UV-radiation fluxes in the range A , while causing practically no changes in the fluxes in the range b . In this case the cloudiness effect could result in a decrease of the effect being studied.

In our opinion, it is most likely that the increase of the scattered UV-radiation flux during this solar eclipse is due to the above-mentioned morning fog, whose occurrence and dissipation corresponded exactly to the time limits of the solar eclipse (see Fig. 2). From a comparison of time behaviors, depicted in Figs. 2 and 4, it follows that the above maximum of the scattered

UV-radiation flux was observed during the fog dissipation (at 9 a.m.) when the optical depth τ of the atmospheric vertical layer rapidly decreased. If it is assumed that the height of the fog layer was about ~ 0.1 km, then, according to estimates made on the basis of data presented in Fig. 2, the quantity τ decreased from 1.3 to 0.3 over a period from 8:45 to 9:00 a.m. But at $\tau = 1$ the scattered radiation flux A_1 in the approximation of single scattering has a well pronounced maximum according to $A_1 \sim \tau e^{-\tau}$ dependence.⁸ This fact enables one to assume that the increase of the scattered UV-radiation flux observed immediately after the eclipse is due to the contribution of single scattered direct solar radiation on the particles of the dissipated fog when its optical depth τ becomes close to unity. In this case the contribution from higher orders of multiple scattering, which only weakly depends on the optical depth of a scattering layer, can not result in the revealed maximum within the range of optical depths that took place during the observations.

4. Conclusion

To summarize, we can state that from the continuous measurements of the sky background flux in the UV-region, made during the morning solar eclipse, an extremely high level of UV-radiation was observed during the first minutes after the termination of the eclipse and then its value gradually relaxed to its normal level. The time behavior of the ratio between the flux obtained during the eclipse, to the flux obtained at the same time the next day, exhibits a well pronounced maximum, which is not related to the decrease of the overall aerosol content during the eclipse.

Simultaneous measurements of the aerosol extinction coefficients in the near-ground atmospheric layer revealed that the detected maximum coincided in time with the fog dissipation formed during the solar eclipse. This fact makes it possible to assume, that the increase in the scattered UV-radiation flux observed immediately after the eclipse is due to the contribution of single scattered solar radiation on the particles of dissipated fog, when its optical depth τ becomes close to unity. In this case the

scattered radiation flux in the approximation of single scattering, A_1 , exhibits a well pronounced maximum according to the relationship $A_1 \sim \tau e^{-\tau}$.

The analysis of the time behavior of meteorological parameters, i.e., the temperature of underlying surface and the calculated values of the atmospheric effective radiation shows that the fog formation in the morning on the 9th of March was most likely caused by the solar eclipse, during the course of which the deficit of incoming solar radiation resulted in the air temperature drop in the middle and upper troposphere. Owing to this fact, the conditions occurred for the formation of the cloudiness of the upper and middle levels, which caused the change of sign of the effective radiation at the underlying surface and, as a result, the formation of the fog.

Acknowledgments

The work has been partly supported by the Russian Foundation for Basic Research (Grant No. 97-05-65994).

References

1. Yu.A. Pkhalagov, V.N. Uzhegov, and U.U. Shchelkanov, *Atmos. Oceanic Opt.* **5**, No. 6, 423–426 (1992).
2. L.T. Matveev, *Manual of General Meteorology. Atmospheric Physics* (Gidrometeoizdat, Leningrad, 1976), 639 pp.
3. I.I. Ippolitov, V.S. Komarov, and A.A. Mitsel, in: *Spectroscopic Methods Used for Atmospheric Sensing*, I.V. Samokhvalov, ed., (Nauka, Novosibirsk, 1985), pp. 4–44.
4. A.A. Eliseev, I.I. Ippolitov, M.V. Kabanov, et al., *Atmos. Oceanic Opt.* **7**, No. 5, 301–302 (1994).
5. A.B. Beletskii, A.V. Mikhalev, and M.A. Chernigovskaya, *Atmos. Oceanic Opt.* **11**, No. 4, 301–306 (1998).
6. G.P. Gushchin and N.N. Vinogradova, *Total Ozone in the Atmosphere* (Gidrometeoizdat, Leningrad, 1983), 231 pp.
7. A.A. Eliseev, I.I. Ippolitov, M.V. Kabanov, et al., *Izv. Vyssh. Uchebn. Zaved., Fizika*, No. 9, 71–74 (1998).
8. V.E. Zuev, and M.V. Kabanov, *Optics of Atmospheric Aerosol* (Gidrometeoizdat, Leningrad, 1987), 254 pp.
9. *The Stratosphere 1981. Theory and Measurements*, Report USA, No. 11, Appendix B., B10–B11 (1981).